

FEA Information Inc.
Global News & Technical Information
Dedicated to the Engineering Community

September 2002



LEAP	ALTAIR-Italy ALTAIR-Western Region USA	DYNAMAX	ANSYS-China
DYNALIS	GISSETA	DYNAmore	FLOTREND
KOSTECH	ERAB	THEME	MFAC
CAD-FEM	Prof Gennaro Monacelli	Dr. David Benson	Dr. Alexey I. Borovkov
Dr. Ted Belytschko	Dr. Taylan Altan	Dr. Bhavin V. Mehta	Prof. Ala Tabiei



FEA Information Inc.

Global News & Industry Information

Volume 2

Issue 9-2002

September

Editor: Trent Eggleston
Technical Writer Arthur B. Shapiro
Technical Writer David Benson
Graphic Designer Wayne Mindle
Feature Director Marsha Victory

Purpose:

The purpose of our publication is to provide technical and industry information

Featured Article

03	September 11 Pentagon Attack Simulations Using LS-DYNA Phase 1 - Mete A. Sozen, Sami A. Kilic and Christoph M. Hoffman
----	---

In This Issue:

07	DesignSpace Speeds Mitroflow International's Development of Pericardial Heart Valves – ANSYS Inc.
10	Website Summary
11	FEA Information Inc. Participant Listing
	Publication: Development of a Coupled Finite Element and Meshfree Method in LS-DYNA – CT Wu

The contents of this publication is deemed to be accurate and complete. However, FEA Information Inc. doesn't guarantee or warrant accuracy or completeness of the material contained herein. All trademarks are the property of their respective owners. This publication is published for FEA Information Inc., Copyright 2002. All rights reserved. Not to be reproduced in hardcopy or electronic format

**September 11 Pentagon Attack Simulations Using LS-DYNA
Phase 1, September 11, 2002, © Copyright**

Mete A. Sozen, Sami A. Kilic and Christoph M. Hoffman

Reproduced with permission of School of Civil Engineering, Purdue University

A special acknowledgement to “Dr. Sami A. Kilic, Purdue University” for the LS-DYNA model development and “Purdue University Aircraft Crash Simulation Team” for the overall effort of the group.

Why?

If any good can come from the events of September 11, it would be to understand in detail what damage occurred, how it occurred, and why it occurred. Then, we should be able to create superior structures that will protect life. By simulating the chilling sequence of events, in this detail, we are able to fashion tools that help decision makers in the future to explore potential disasters before they happen.

Problem Statement: Simulate as faithfully as possible the effects of crashing an air frame loaded with fuel (simulating a Boeing 757) into a reinforced concrete frame similar to the one supporting the Pentagon building. In particular, model the columns to have properties reproducing the behavior of spirally reinforced columns including the difference in material response of the concrete within and outside the spiral reinforcement.

Purpose of the Effort: Use the physically correct simulation results as input to animations and visualizations to produce a vivid reenactment of the impact of the aircraft on the Pentagon building and provide the larger team with the necessary data to construct these using 3D Studio Max, AutoCAD, and research tools.


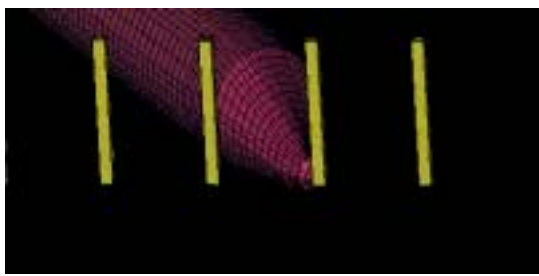
Problem Formulations: Several problem formulations were investigated with the results sketched by the animations below. A basic hypothesis, informally confirmed with engineers knowledgeable in this subject, is that the bulk of the impact damage is due to the body of fuel in the wing and center tanks. Most of the aircraft structure is light-weight low-mass, and relatively low strength, with the exception of the wheel undercarriage. The experiments are

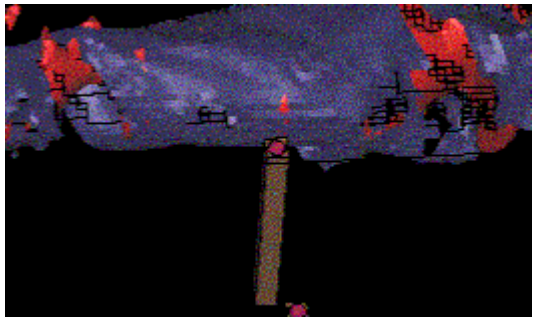
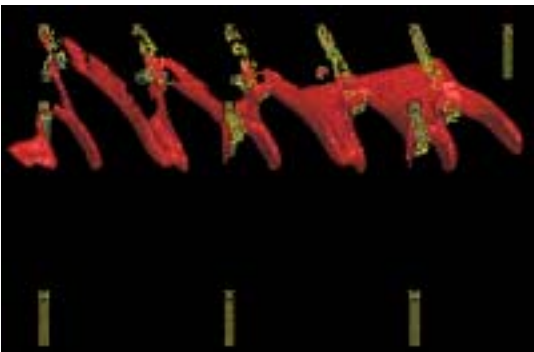
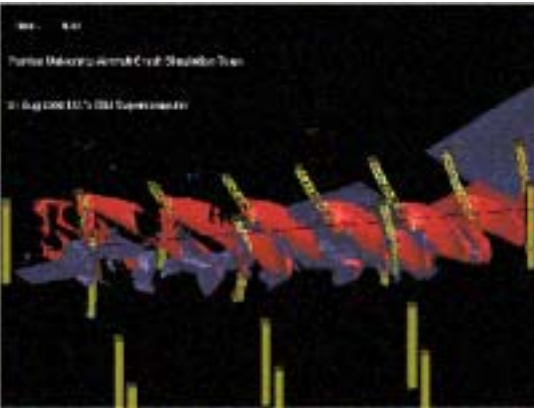

1. A single body of fluid hits a single column. The purpose of this simulation is to understand the response of a reinforced concrete column subjected to high-speed impact of the fuel in the aircraft tanks. In particular, the relationship between the impact velocity of the fluid and the acceleration of the column has been studied.
2. The body of the aircraft hits a single row of columns. The columns model the structural properties of the first-story columns in the Pentagon, including the reinforcing bars and the material difference between the column core and the column facing. The body is shredded as it impacts the structure, confirmed by aeronautical engineers to be plausible.
3. The fuel tank hits three rows of columns. The wing enclosure breaks open and the fluid spills. Wings are modeled without ribs, leading to a balloon effect.
4. The right-wing fuel tank hits the first three rows of columns. The fuel is modeled as fluid, and the problem is a mixed arbitrary Euler-Lagrange mesh formulation. The fuel tank disintegrates, and the fuel disperses into the structure. This time, the wing has ribs and the break-up is realistic.

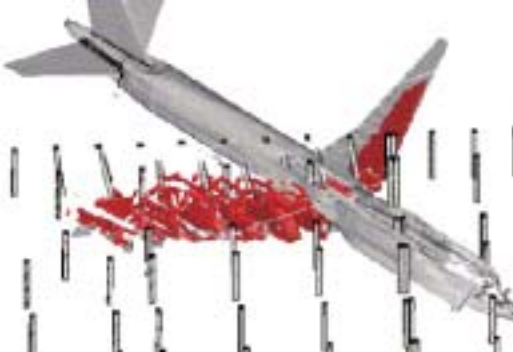
5. The fuel fluid hits the columns and destroys those in the first two rows. This simulation does not include a wing enclosure and so can be used to better understand the effect of the wing strength on the fuel dispersal.
6. Run on the IBM Regatta machine. This machine can run a heavier grade of LS-Dyna and therefore allows us to simulate a more detailed model. This is a brief run.
7. Full model run, coarse model formulation, run on the IBM Regatta. Model includes all columns in the simulated frame and the complete aircraft. The model size is approximately 300,000 nodes. The run took about 24 hours for 40 frames covering 0.2 sec real time.
8. Full model run, detailed model formulation, run on the IBM Regatta. Model has 1,000,000 nodes. With 50 frames computed in close to 68 hours, the simulation covers 0.25 sec real time. Several observations stand out:
 - o The simulation demonstrates that the number of columns destroyed in the facade of the building does not have to correspond to the wing span. The tips of the wings, having less mass, are cut by the columns rather than the wing cutting the columns.
 - o The simulation suggests that the reinforced concrete column core will cut into the fuselage until the fuel depot reaches it, at which time the column is destroyed.
 - o The simulation shows the deceleration of the plane after impact as witnessed by the buckling of the fuselage near the tail structure.

Simulation Parameters: The simulation uses adaptive time stepping which averages to approximately 0.000001sec time steps. We generate snapshots approximately 0.005sec. The airplane is assumed to arrive with an estimated initial velocity of 800 ft/sec. Penetration to column row 4 takes approximately 0.1sec

The Animations can be viewed at www.cs.purdue.edu/homes/cmh/simulation *

	Animations*	Image Preview	Animation Image Size	Problem Size (nodes)	Compute Time
1.	Single Column Pentium 4		13.2 MB	100 K	10 hours
2.	Aircraft Body Pentium 4		2.7 MB	50 K	7 hours

3.	<p>Wing w/o ribs</p> <p>IBM Nighthawk2 16 processors</p>		All Objects	<p>Fluid Tank Enclosure</p>	<p>Columns Close-up</p>
4.	<p>IBM Nighthawk 16 processors</p>			500 K	106 hours
5.	<p>IBM Regatta 8 RISC processors</p>		close-up	1.2 M nodes	
6.	<p>IBM Regatta coarse model</p>		Low-speed Replay	300 K nodes	<p>24 hours 0.2 sec real time</p>

7.	IBM Regatta detailed model		Low-speed Replay Frame 50 big and small	1 M nodes	68 hours 0.25 sec real time
----	----------------------------	---	--	-----------	---------------------------------------

The Larger Team and Responsibilities

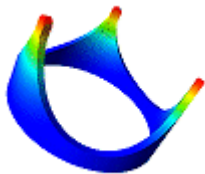
Project Conception	Mete Sozen	Engineering Models	Sami Kilic, CE
Simulation Setups	Sami "Dr. Click" Kilic	Scientific Supervision	Mete Sozen, CE
Infrastructure Support	James Bottum Ahmed Sameh	Supercomputer Runs	William Whitson, ITaP
Project Direction	Christoph Hoffmann	Animation	Voicu Popescu, CS
Mesh Generation	Christoph Hoffmann, CS, CRI	Story Board	Scott Meador, CGT
Graduate Students	Amit Chourasia, CGT Hendry Lim, CS		

DesignSpace Speeds Mitroflow International's Development of Pericardial Heart Valves



Reproduced with Permission of ANSYS Inc.

Heart patients with deteriorating heart valves have benefited from Mitroflow International's development of pericardial heart valves-prostheses that use bovine tissue rather than composite metals as moving parts. Mitroflow first developed these unique heart valve designs in 1982 for patients that wish or need to avoid the anti-coagulant drug therapy typically associated with the implantation of mechanical valves. Patients with pericardial heart valves need not take any medication nor suffer the side effects of drug therapy. Likely candidates for treatment with a Mitroflow pericardial heart valve include women of child-bearing age, older patients, and those for whom mechanical valves and the associated drug therapy is not an acceptable option.



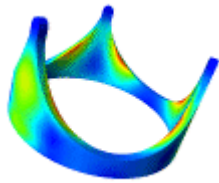
Recently, engineers at Mitroflow, based in Richmond, Canada (B.C.), began examining engineering software that would help reduce design cycles as well as improve the performance and longevity of the implanted valves. Regulatory agencies, such as the U.S. Food and Drug Administration, have stringent testing requirements for products like these. Mitroflow engineers realized that they needed to focus on the traditional three-year design cycle and evaluate simulation software that could assist them during initial design rather than as a means for final prototyping. They now use DesignSpace for Autodesk Mechanical Desktop from ANSYS Inc. (Canonsburg, PA).



Constructing a Better Heart Valve

Mitroflow's pericardial heart valve uses tissue that is harvested from the pericardial sac of cows. A single flap of bovine tissue is fashioned into the valve leaflets, which open and close as the heart beats to expel blood. The valve leaflets, which vary in size and thickness depending on the size of the patient's heart valve to be replaced, are mounted on the outside of the stent, a solid structure which holds the valve leaflets for attachment to the patient's heart tissue. The stent is constructed from an acetate homopolymer material that is selected for its "low creep" properties. The stent is an important design component and must be designed for maximum working orifice area while maintaining structural strength. A sewing ring,

which is molded from medical grade silicon, connects and conforms to the patient's cardiac tissue. A tightly woven medical grade Dacron(r) fabric is used to cover both the sewing ring and the stent.



The stent is a valve component of design interest for improving the durability and longevity of the valves once implanted, according to Jennifer Arntorp, Engineering Manager at Mitroflow. Studies of previous heart valve designs showed an average life cycle of about 10 years (The current Model 12 valves have been tested in-house (in vitro) to last for almost 20 years without deterioration, with 10 to 15 years being the expected (in vivo) life span). Mitroflow engineers have two main objectives in the design of their next generation heart valve: (1) redesign the stent to increase the expected life of the implanted valve to between 15 and 20 years; (2) shorten the design cycle for the product, which traditionally has been as long as three years. As part of this effort, Mitroflow explored the use of simulation technology to examine the strength, flexibility, and deformation of the stent component.

Practical Simulation Software

According to Mark Chaplin, Engineering Technologist at Mitroflow, the company had evaluated traditional finite element analysis (FEA) packages as a way to shorten product development cycles and improve product performance. The company found traditional FEA software to be expensive and generally not easy to use. "We've reviewed other packages, and walked away from them in frustration," Chaplin explained. "When we evaluated DesignSpace (for Mechanical Desktop), the choice became clear. The software is very easy to use and suitable for the type of design work we do."

As part of the DesignSpace evaluation, which was completed during a free 30-day trial, Mitroflow took steps to validate DesignSpace results against known testing responses for existing designs.

"The DesignSpace results were within 10 percent of our actual testing results," Chaplin said. "That's better than we expected from the software and good enough to make initial prototype design decisions. We're 100-percent confident in the software results, and are now using the software as a regular design tool."

Improving the Design Process

In pursuing the company's design objective of increasing valve longevity, Mitroflow is using DesignSpace to examine the flexibility of the valve stent—specifically, deflection in the stent posts. The secondary objective of design simplification to make the manufacturing process easier and more cost-effective is also part of this work. All DesignSpace analyses were done inside Mechanical Desktop on a Pentium 120 MHz computer with 64 MB of RAM running Windows 95.

"We've used DesignSpace to look at different prototypes before choosing the design to pursue," Arntorp noted. "DesignSpace allowed us to run different scenarios and make decisions that were necessary for an optimized heart valve design."

In just a couple months, Mitroflow's project team has finalized designs for two sizes of the next pericardial heart valve model. Mitroflow produces six different sizes of valves for each model to accommodate the varying heart sizes in human beings. Heart size varies with physical stature and, for the most part, coincides with the size of a human fist. In the past, company engineers could spend as long as six months on one size of a model.

"Before using DesignSpace, developing a design was really trial and error. We'd have an idea, do some rough hand calculations and then go through a prototype testing cycle. With DesignSpace, we have more confidence in our initial prototypes," Arntorp said. "DesignSpace will shorten our product development life cycles and improve the performance of our products. It already has!"

Like all medical device manufacturers, Mitroflow must meet stringent regulatory testing and approval requirements. With heart valves, this approval process takes anywhere from nine months to a couple of years, so any time savings that can be realized are extremely important.

DesignSpace provides an additional benefit to Mitroflow in the design and manufacture of products in a tightly regulated market. DesignSpace results provide evidence and add credibility to Mitroflow's regulatory submissions-another reason why Mitroflow is taking DesignSpace to heart.



**FEA Information August News archived on the site News Page
www.feainformation.com**

August 05:

- **Fujitsu:** upgrades to its PRIMEPOWER™ family of Solaris™ compatible servers with the global introduction of seven enhanced models.
- **LMS Test.Lab** is an integrated software suite for Noise & Vibration Testing and Engineering
- **Metal Forming Analysis Corp.** located in Canada, supplies a full range of services for the sheet metal forming analysis industry.

August 12

- **AMD Mobile AMD Athlon™ XP Processor Extreme Performance** for Windows® XP
- **CEI EnLiten** is a 3D geometry player for viewing, analyzing and manipulating complex visualization scenarios
- **Dynamax**, located in Michigan, for LS-DYNA sales, training, support & consulting

August 19

- **ANSYS ANSYS/Multiphysics™** integrates the best structural, thermal, CFD, acoustic and low-/highfrequency electromagnetic simulation capabilities in one software bundle.
- **ERAB**, located in Sweden, LS-DYNA sales, distribution and consulting.

August 26

- **MSC.Nastran** is a computer aided engineering (CAE) tool for critical engineering computing needs to produce safe, reliable, faster and optimized designs.
- **JRI JMAG STUDIO** analysis selectable either in the frequency domain (Finite Element Method) or the time domain (Finite Difference Time Domain) depending on the problem.
- **THEME Engineering**, located in Korea for LS-DYNA sales, consulting, training and support

2002	EVENTS/CONFERENCES
Oct. 03 - 04	Engin Soft Conference Users Meeting - Italy
Oct 08	OASYS LS-DYNA Update Meeting - UK
Oct. 9-11	CAD-FEM Users Meeting - International Congress on FEM Technology, Germany.
Oct. 10-13	10th Foresight Institute Conf. on Molecular Nanotechnology in Bethesda, MD, USA.
Oct 24 - 25	Japanese LS-DYNA & JMAG Users Conference at the Hilton Nagoya.
Oct 28	Korean LS-DYNA Users Conference – THEME Engineering
Nov. 28 & 29	LMS Conference for Physical and Virtual Prototyping,, Stuttgart, Germany
Dec 18 - 21	HiPC 2002 will be held in Bangalore, India known as the Silicon Valley of India.
2003	
Feb 18	Fujitsu LS-DYNA seminar at Makuhari System Laboratory, Makuhari, Japan
May 19-21	BETECH Detroit, USA - 15th Int'l Conference on Boundary Element Technology
May 22 - 23	4th European LS-DYNA Conference will be held in ULM,
June 17-20	The Second M.I.T. Conference on Computational Fluid and Solid Mechanics , taking place at Massachusetts Institute of Technology Cambridge, MA.,USA

FEA Information Inc. Commercial & Educational Participants

Headquarters	Company	
Australia	Leading Engineering Analysis Providers	www.leapaust.com.au
Belgium	LMS, International	www.lmsintl.com
Canada	Metal Forming Analysis Corp.	www.mfac.com
China	ANSYS Beijing	www.ansys.com (link on international)
France	Dynalis – Cril Technology Simulation	www.criltechnology.com
Germany	DYNAMore	www.dynamore.de
Germany	CAD-FEM	www.cadfem.de
India	GissEta	www.gisseta.com
Italy	Altair Engineering srl	www.altairtorino.it
Japan	The Japan Research Institute, Ltd	www.jri.co.jp
Japan	Fujitsu Ltd.	www.fujitsu.com
Korea	THEME Engineering	www.lsdyna.co.kr
Korea	Korean Simulation Technologies	www.kostech.co.kr
Russia	State Unitary Enterprise - STRELA	www.ls-dynarussia.com
Sweden	Engineering Research AB	www.erab.se
Taiwan	Flotrend Corporation	www.flotrend.com
UK	OASYS, Ltd	www.arup.com/dyna
USA	Livermore Software Technology	www.lstc.com
USA	Engineering Technology Associates	www.eta.com
USA	ANSYS, Inc	www.ansys.com
USA	Hewlett Packard	www.hp.com
USA	SGI	www.sgi.com
USA	MSC.Software	www.mssoftware.com
USA	EASi Engineering	www.easiusa.com
USA	DYNAMAX	www.dynamax-inc.com
USA	CEI	www.ceintl.com
USA	AMD	www.amd.com
USA	INTEL	www.intel.com
USA	Dr. T. Belytschko	Northwestern University
USA	Dr. D. Benson	Univ. California – San Diego
USA	Dr. Bhavin V. Mehta	Ohio University
USA	Dr. Taylan Altan	The Ohio State U – ERC/NSM
USA	Prof. Ala Tabiei	University of Cincinnati
Russia	Dr. Alexey I. Borokov	St. Petersburg State Tech. University
Italy	Prof. Gennaro Monacelli	Prode – Elasis & Univ. of Napoli, Federico II

DEVELOPMENT OF A COUPLED FINITE ELEMENT AND MESH-FREE METHOD IN LS-DYNA

Cheng-Tang Wu ¹, Mark E. Botkin ² and Hui-Ping Wang ²

¹ Livermore Software Technology Corporation
7374 Las Positas Road
Livermore, CA 94550
ctwu@lstc.com

² GM R & D Center
Mail Code 480-106-256
Vehicle Analysis and Dynamics Lab
Warren, MI 48090-9055
mark.e.botkin@gm.com, hui-ping.wang@gm.com

Keywords: mesh-free; finite element; integration constraint

Abbreviations:

RKPM : reproducing kernel particle method
EFG : element-free Galerkin
SCNI : stabilized conforming nodal integration

ABSTRACT

A coupled finite element and mesh-free method for the solid and structure analysis has been proposed. This method is developed to minimize the mesh distortion problems encountered in the finite element analysis and to reduce the high CPU cost associated with the mesh-free computation.

To couple the mesh-free method with the LS-DYNA, an *interface constraint* has been developed. This *interface constraint* is introduced onto the interfaces between finite element and mesh-free zones, and mesh-free and mesh-free zones. The completeness condition is imposed in the solution approximation to achieve the desired consistency across the interfaces.

To satisfy the linear exactness in the mesh-free Galerkin approximation of the Dirichlet boundary value problem, two *integration constraints* have been developed. A local boundary integration scheme has been proposed to satisfy the *first integration constraint* and to eliminate the possible hourglass modes. The *interface constraint* is further extended to the essential boundaries to meet the *second integration constraint* and to reduce the computation time on the imposition of essential boundary conditions. Several examples are solved to evaluate the numerical performance.

INTRODUCTION

Structures subjected to severe material distortion commonly exist in survivability, safety and manufacturing related applications in the defense, aerospace, and automotive industries. Typical examples in the automotive industry are vehicle crashes in frontal and side impact, fuel tanks subjected to impact load, and metal parts manufactured by forging or stamping processes. Despite its success in the analysis of geometric and material nonlinear behavior in structures and solids, the widely used finite element method exhibits a number of shortcomings in handling design problems involving large deformation, high gradients, localization, or moving discontinuities. These difficulties are partially due to the regularity requirement of mesh discretization. In the industrial community, this becomes one of the most challenging tasks in numerical simulations.

In recent years, classes of mesh-free methods have been developed for specific applications [1, 2, 13]. In these methods, the domain of interest is discretized by a scattered set of points. The uniqueness of the mesh-free methods is due to the development of new interpolation/shape functions that allow the interpolation of field variables to be accomplished at a global level without the usage of meshes. These methods are ideal for hp-adaptivity, fracture problems, multiple-resolution analysis, and large deformation problems. However, most of the mesh-free methods consume considerably higher CPU time than the finite element methods.

To resolve this problem, several mixed finite element and mesh-free methods have been proposed [3, 12, 15]. The objective is to use the advantages of each method. Belytschko et al. [3] first introduced a transit element that is of the size of one finite element and the linear interpolation of mesh-free. Wagner and Liu [16] proposed a corrected collection method. Those methods require an extra degree of freedoms for the coupling of the conventional finite element method and mesh-free method. Huerta et al. [12] revised Belytschko's approach and propose a mixed hierarchical approximation based on the element-free Galerkin method [2].

In this paper, we present a coupled finite element and mesh-free method in conjunction with the LS-DYNA [11] code for explicit dynamic analysis. This paper is organized as follows: In first part, the development of the coupled finite element and mesh-free method is described, and the required interface constraints and consistency conditions across interfaces are discussed. The second part presents the coupled finite element and mesh-free formulation for explicit dynamic analysis. Two integration constraints are developed to satisfy the linear exactness in the mesh-free Galerkin approximation of the Dirichlet boundary value problem. Numerical results are presented in the third part to demonstrate the effectiveness of this development, followed by conclusions and discussions.

A COUPLED FINITE ELEMENT AND MESH-FREE METHOD

To reduce the mesh distortion problems in standard finite element analysis, the mesh-free computation is added into the existing finite element based analysis model. The coupling of this mesh-free computation should be computationally efficient, with few modification of the original analysis model, and numerically consistent.

In conventional coupling methods, a layer of finite elements is added onto the interface between each finite element and mesh-free zone. The shape functions of those interface elements are comprised of the standard finite element and conventional mesh-free shape functions with the completeness condition imposed to satisfy the consistency. Nevertheless, these methods still require the structured interface elements and their performance are affected by the elements regularity.

To avoid the structured interface element requirement, an *interface constraint* is proposed. The idea of this proposed *interface constraint* is to introduce a strip of finite element 'nodes' (instead of using a layer of structured interface elements) on the interface between finite element and mesh-free zones, and mesh-free and mesh-free zones as shown in Figure 1. These additional nodes are taken to be the same nodes from the finite element based analysis model and do not require an extra degree of freedoms. As a result, the computation preserves the mesh-free unstructured characteristics, modification effort for the standard finite element based analysis model is minimized, and the computation can be efficient.

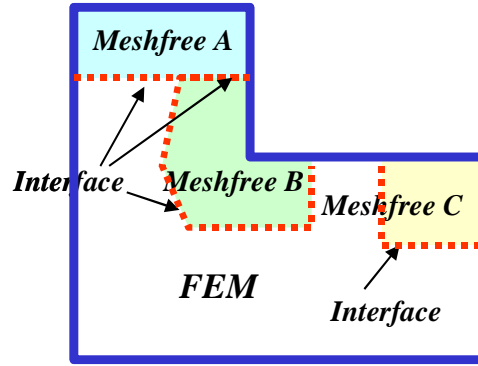


Figure 1. A two-dimensional FEM analysis model with three added mesh-free computation zones: Mesh-free A, B and C and four corresponding interfaces.

Derivation of the coupled finite element and mesh-free method is presented in following section. At first, the mesh-free approximations are constructed based on the framework of moving least-squares interpolation. The element-free Galerkin method (EFG) [2] and the reproducing kernel particle method (RKPM) [13] are two representatives of moving least-squares approximation. In this study, we formulate the mesh-free approximation by the RKPM. According to the proposed idea, the discrete solution approximation at a point \mathbf{x} is obtained as

$$u_i(\mathbf{x}) \approx u_i^h(\mathbf{x}) = \begin{cases} \sum_{\mathbf{x}_L \in \Omega_{FEM}}^{KP} \Phi_L^{[m]}(\mathbf{x}; \mathbf{x} - \mathbf{x}_L) d_{iL}; \forall \mathbf{x} \in \Omega_{FEM} \subset \mathbf{R}^d \\ \sum_{\mathbf{x}_I \in \Omega_{Meshfree}}^{NP} \bar{w}_a^{[n]}(\mathbf{x}; \mathbf{x} - \mathbf{x}_I) d_{iI} + \sum_{\mathbf{x}_L \in \Gamma_{Interface}}^{MP} \Phi_L^{[m]}(\mathbf{x}; \mathbf{x} - \mathbf{x}_L) d_{iL}; \forall \mathbf{x} \in \Omega_{Meshfree} \subset \mathbf{R}^d \end{cases} \quad (1)$$

where Ω_{FEM} denotes the sub-domain for the finite element computation and $\Omega_{Meshfree}$ is the sub-domain for mesh-free computation. $\Omega := \Omega_{FEM} \cup \Omega_{Meshfree}$ is a bounded domain in \mathbf{R}^d and $\Gamma_{Interface} := \Omega_{FEM} \cap \Omega_{Meshfree}$ is the interface between the finite element and mesh-free sub-domains or the interface between any two mesh-free sub-domains.

$\bar{w}_a^{[n]}$ is called the reproducing kernel function, and is usually expressed by a linear combination of n -th order local basis functions and a compact support kernel function; $[n]$ denotes the order of basis functions and 'a' is the support size of the kernel. $\Phi_L^{[m]}$ is the standard finite element shape function with order of interpolation $[m]$. NP is the total number of mesh-free particles that influence the solution at point \mathbf{x} . KP is the total number of the finite element nodes per element when point \mathbf{x} is located inside the finite element zones. d_{iI} is the coefficient of the approximation, and in general is not equivalent to the physical displacement. MP is the total number of the finite element nodes on the interface that influence the approximation.

Using the following reproducing conditions [14], one can restore the polynomials to a specific order by requiring the zero-th moment [14] to be one, and the higher order moments to be zero. The reproducing condition also refers to the completeness condition of an approximation, and is important for the convergence in the Galerkin methods.

$$\sum_{\mathbf{x}_I \in \Omega_{Meshfree}}^{NP} \bar{w}_a^{[n]}(\mathbf{x}; \mathbf{x} - \mathbf{x}_I) x_{1I}^i x_{2I}^j + \sum_{\mathbf{x}_J \in \Gamma_{Interface}}^{MP} \Phi_J^{[m]}(\mathbf{x}; \mathbf{x} - \mathbf{x}_J) x_{1J}^i x_{2J}^j = x_1^i x_2^j, \quad i + j = 0, \dots, n \quad (2)$$

It is important to notice that, in most cases, the order of finite element interpolation $[m]$ is chosen to be the same as the reproducing order $[n]$, and the approximation is continuous everywhere in $\Omega_{Meshfree}$. If the reproducing order $[n]$ is larger than the finite element interpolation order $[m]$, i.e. $n > m$, then continuity is preserved only in $\Omega_{Meshfree} \setminus \Gamma_{Interface}$. Thus, discontinuities in the approximation are induced along $\Gamma_{Interface}$.

Satisfaction of the reproducing conditions in Equation (2) leads to the following coupled finite element and mesh-

free solution approximation with the n -th order solution completeness.

$$u_i^h(\mathbf{x}) = \sum_{x_I \in \Omega_{Meshfree}}^{NP} \tilde{\Psi}_I(\mathbf{x}) d_{iI} + \sum_{x_J \in \Gamma_{Interface}}^{MP} \Phi_J^{[m]}(\mathbf{x}) d_{iJ} = \sum_{x_I \in \Omega_{Meshfree}}^{NP} \hat{\Psi}_I(\mathbf{x}) d_{iI} \quad (3)$$

where

$$\begin{aligned} \tilde{\Psi}_I(\mathbf{x}) = & \sum_{x_I \in \Omega_{Meshfree}}^{NP} \{ \mathbf{H}^{[n]\Gamma}(\mathbf{0}) \mathbf{M}^{[n]\Gamma'}(\mathbf{x}) \mathbf{H}^{[n]}(\mathbf{x} - \mathbf{x}_I) \\ & - \sum_{x_J \in \Gamma_{Interface}}^{MP} \mathbf{H}^{[n]\Gamma}(\mathbf{x} - \mathbf{x}_J) \mathbf{M}^{[n]\Gamma'}(\mathbf{x}) \mathbf{H}^{[n]}(\mathbf{x} - \mathbf{x}_I) \Phi_J^{[m]}(\mathbf{x}; \mathbf{x} - \mathbf{x}_J) \} w_a(\mathbf{x} - \mathbf{x}_I) d_{iI} \end{aligned} \quad (4)$$

$\tilde{\Psi}_I$ is the reproducing kernel function corresponding to the mesh-free node I , and $\Phi_J^{[m]}$ is the standard finite element shape function associated with the finite element node J . $\hat{\Psi}_I$ is the modified coupled finite element and mesh-free shape function for the node I .

It has been shown by Wu [18] that for Equation (1) to be conforming across any interface, a necessary condition is required which is

$$\tilde{\Psi}_I(\mathbf{x}) = 0 \text{ for all nodes } \{ I : \text{supp}(\Psi_I) \cap \Gamma_{Interface} \neq \emptyset \} \text{ and } \mathbf{x} \in \Gamma_{Interface} \quad (5)$$

We call Equation (5) the **interface constraint**. In other words, the shape functions on the interface between the finite element and mesh-free zones are reduced to standard finite element shape functions and pose the Kronecker delta property. Therefore, there is no non-conforming problem for the shape functions across the interface.

When $\mathbf{x} \in \Omega_{Meshfree} \setminus \Gamma_{Interface}$, and $n = m$ in Equation (2), the solution approximation will still meet the m th-order reproducing conditions.

FORMULATION FOR EXPLICIT DYNAMIC ANALYSIS

In this section, solution of the governing equations using the proposed coupled finite element and mesh-free approximation is achieved under the framework of the Galerkin weighted residual method. To satisfy the linear exactness in the Galerkin approximation, two integration constraints are introduced. A new mesh-free approximation is developed based on these two integration constraints, and a spatial integration scheme is introduced for the domain integration.

Recall the Lagrangian partial differential equation of motion

$$\rho \ddot{\mathbf{u}} = \nabla \cdot \boldsymbol{\sigma} - \mathbf{f}_b \text{ in } \Omega, \Omega = \Omega_{FEM} \cup \Omega_{Meshfree} \quad (6)$$

with the divergence operator ∇ , the body force \mathbf{f}_b , and the essential and natural boundary conditions

$$\begin{aligned} \mathbf{u} &= \mathbf{u}_0 \text{ on } \Gamma_g \\ \boldsymbol{\sigma} \cdot \mathbf{n} &= \mathbf{h} \text{ on } \Gamma_h \end{aligned} \quad (7)$$

and with initial conditions

$$\begin{aligned} \mathbf{u}(\mathbf{X}, 0) &= \mathbf{u}^0(\mathbf{X}) \\ \dot{\mathbf{u}}(\mathbf{X}, 0) &= \dot{\mathbf{u}}^0(\mathbf{X}) \end{aligned} \quad (8)$$

The left side of Equation (6) is the material time derivative and will involve convective terms if the Eulerian kernel functions are used. To avoid the tensile instability caused by the Eulerian kernel functions [4], the Lagrangian kernel functions are implemented in this study.

To solve this set of partial differential equations with the Galerkin method (which is considered as standard for the development in the finite elements based on the displacement method), the equilibrium in its strong form of Equations (6)-(8) is weighted with some test functions defined by $W = \{w/w \in L^2(\Omega), w = 0 \text{ on } \Gamma_g\}$. The corresponding weak form of Equation (6)-(8) becomes:

$$\int_{\Omega_x} \rho w \ddot{u} d\Omega = \int_{\Omega_x} w \cdot \nabla \cdot \sigma d\Omega - \int_{\Omega_x} w \cdot f_b d\Omega - \int_{\Gamma_h} w \cdot h d\Gamma \quad (9)$$

with

$$\begin{aligned} u(X, 0) &= u^0(X) \\ \dot{u}(X, 0) &= \dot{u}^0(X) \end{aligned} \quad (10)$$

The next step in the discretization is to choose a finite dimensional subspace $U^h \subset U$ with basis $\hat{\Psi}_I (I = 1 \dots n)$. $\hat{\Psi}_I (I = 1 \dots n)$ are the shape functions obtained from Equation (1). To this end, the basis of weighted functions is chosen to be the same as the trial functions after the spatial discretization. Since we choose the weighted functions to be in $H_0^1(\Omega)$, we can integrate by parts and obtain the discrete Galerkin weighted residual formulation. The references for the detailed derivation of weak equations and the imposition of essential boundary conditions using kinematically admissible mesh-free shape functions can be found in [5-7, 17]. Following the derivation for explicit time integration, the equations to be solved have the form

$$\delta \hat{u}^T A^{-T} M A^{-1} \hat{u} = \delta \hat{u}^T A^{-T} R^{int} \quad (11)$$

where

$$\begin{aligned} \ddot{u}_I &= [\ddot{d}_{1I}, \ddot{d}_{2I}]^T \\ M_{IJ} &= \int_{\Omega_x} \rho \hat{\Psi}_I(x) \hat{\Psi}_J(x) d\Omega = \int_{\Omega_x} \rho^0 \hat{\Psi}_I(X) \hat{\Psi}_J(X) d\Omega \\ R_I &= \int_{\Omega_x} B_I^T(x) \cdot \sigma d\Omega - [\hat{\Psi}_I(x) h] \Big|_{\Gamma_h} - \int_{\Omega_x} \hat{\Psi}_I(x) f_b d\Omega \end{aligned} \quad (12)$$

and

$$\hat{u} = Au; A_{IJ} = \hat{\Psi}_J(X_I) \quad (13)$$

Usually, the numerical integration in Equation (11) is evaluated by Gauss quadrature using the so-called background mesh. However, the Gauss integration method fails to satisfy the linear exactness in the mesh-free Galerkin approximation of a second-order partial differential equation. Moreover, a higher order quadrature rule is often required for better accuracy, and this is one of the major causes of high CPU consumption in mesh-free methods. For convergence reasons, an *integration constraint* is required as a necessary condition for the linear exactness in the mesh-free Galerkin approximation of Dirichlet boundary value problems [9, 10]. Here, we call this the *first integration constraint* and it is given by

$$\int_{\Omega} B_I^T d\Omega = 0 \text{ for all interior nodes } \{I : \text{supp}(\tilde{\Psi}_I) \cap \Gamma_{\text{boundary}} = 0\} \quad (14)$$

or in the discrete form,

$$\sum_{J=1} \nabla \hat{\Psi}_I(\mathbf{x}_J) A_J = \mathbf{0} \quad \text{for all interior nodes } \{I : \text{supp}(\tilde{\Psi}_I) \cap \Gamma_{\text{boundary}} = \emptyset\} \quad (15)$$

where \mathbf{B}_I is the gradient matrix; A_J is the weight of the domain integration point.

To meet this integration constraint, a stabilized conforming nodal integration method (SCNI) [9, 10] has been proposed. This method was originally designed as a strain smoothing stabilization in the strain localization analysis [8]. The method was further extended to minimize the integration errors and improve the computation inefficiency in the conventional mesh-free higher-order Gauss integration method.

From our numerical studies we observed that SCNI fails to satisfy the linear exactness in the cases when the supports of inner nodes cover the essential boundary nodes. In other words, the solution fails to display a linear displacement field in the Galerkin approximation of Dirichlet boundary value problem if $\exists \{x_I\}$ for $\{I : \text{supp}(\Psi_I) \cap \Gamma_g \neq \emptyset\}$. Therefore the satisfaction of *first integration constraint* is said to have passed a ‘weak’ linear exactness test. Wu [18] has further proved that for the mesh-free solution to satisfy the linear exactness test, an additional integration constraint is required.

$$\sum_{M=1} \hat{\Psi}_M(\mathbf{x}_N) \mathbf{x}_N = \mathbf{0} \quad \forall \mathbf{x}_N \in \Gamma_g \quad \text{and} \quad \mathbf{x}_M \in \Omega_{\text{Meshfree}} \setminus \Gamma_g \quad (16)$$

We call Equation (16) the *second integration constraint*. It can be proved that the conventional mesh-free shape function and the coupled shape function $\hat{\Psi}_I$ in Equation (3) do not meet this requirement and therefore fails to satisfy the linear exactness in the mesh-free Galerkin approximation of Dirichlet boundary value problem. Moreover, the calculation of Equation (11) and the generalized displacement in Equation (13) by the conventional mesh-free approximation requires additional efforts for the matrix multiplication during each time step. Therefore, much higher computation time is expected in the implicit calculation. This is another major cause of high CPU usage for the mesh-free method.

To resolve the problem in the violation of the *second integration constraint*, and to improve the inefficiency in the calculation of Equations (11) and (13), the *interface constraint* concept is extended to the imposition of essential boundary conditions and contact conditions. By further extending similar constraint from interface to boundary, the solution approximation in the mesh-free zone is modified as

$$u_i^h(\mathbf{x}) = \sum_{x_I \in \Omega_{\text{Meshfree}}}^{NP} \bar{w}_a^{[m]}(\mathbf{x}; \mathbf{x} - \mathbf{x}_I) d_{iI} + \sum_{x_L \in \Gamma_{\text{boundary}}}^{MP} \Phi_L^{[m]}(\mathbf{x}; \mathbf{x} - \mathbf{x}_L) d_{iL} = \sum_{x_I \in \Omega_{\text{Meshfree}}}^{NP} \bar{\Psi}_I(\mathbf{x}; \mathbf{x} - \mathbf{x}_I) d_{iI} \quad (17)$$

$, \forall \mathbf{x} \in \Omega_{\text{Meshfree}}; \Gamma_{\text{interface}} \subset \Gamma_{\text{boundary}}$

It has been proven [18] that this new solution approximation satisfies the *second integration constraint*.

Another major shortcoming of the SCNI method is its inability to couple the mesh-free method with the finite element method. This is because the SCNI method is a nodal integration method, and all the quantities are computed and assigned to the nodes. As a result, internal variables such as strains and stresses evaluated at the interface nodes between finite element and mesh-free zones, and mesh-free and mesh-free zones are inconsistent. Moreover, from our numerical studies, it is also shown that the SCNI method displays hourglass modes when the support size is small or a high order basis function is adopted in the analysis.

In order to avoid the undefined nodal quantities on the interface and also to eliminate possible hourglass modes observed in the SCNI method, a modified local boundary integration method is introduced in this research for the domain integration. This method is equivalent to the two points Gauss integration with local boundary integration performed on each gauss point. For a more detailed derivation on the modified local boundary integration method see Wu [18].

To introduce the strain smoothing formulation into the Galerkin approximation, the mixed variational principle based on an assumed strain method is considered [9, 10]. Substituting the displacement and smoothed strain

approximations into Equation (11) and performing the local boundary integration method [18], the discrete system equation becomes

$$\mathbf{M}\ddot{\mathbf{u}} = \mathbf{f}^{ext} - \mathbf{f}^{int}(\hat{\nabla}\mathbf{u}_i^h) \quad (18)$$

In the explicit dynamic analysis, a lumped mass matrix is considered for the computation efficiency. In this study, a row-sum method is used for the construction of the lumped mass matrix. Recall the consistent mass matrix in Equation (12), and perform the row-sum method, the diagonalized mass vector is given as

$$M_I^{lump} = \sum_{J=1} M_{IJ} = \int_{\Omega_x} \rho^0 \bar{\Psi}_I(\mathbf{X}) \sum_{J=1} \bar{\Psi}_J(\mathbf{X}) d\Omega = \int_{\Omega_x} \rho^0 \bar{\Psi}_I(\mathbf{X}) \quad (19)$$

The discrete form of \mathbf{f}_I^{int} in Equation (18) is

$$\mathbf{f}_I^{int}(\hat{\nabla}\mathbf{u}_i^h) = \sum_{IE=1}^{NE} \sum_{g=1}^{nint} \bar{\mathbf{B}}_I^T(\mathbf{X}_g) \bar{\mathbf{G}}^T \cdot \bar{\boldsymbol{\sigma}}(\bar{\mathbf{F}}(\mathbf{x}_g)) \bar{\mathbf{J}}(\mathbf{X}_g) A_g \quad (20)$$

where $\bar{\mathbf{G}}^T$ is the transform matrix of the inverse of the smoothed deformation gradient for the usage of Lagrangian kernel function. For example, in a two-dimensional problem

$$\bar{\mathbf{G}}^T = \begin{bmatrix} \bar{F}_{11}^{-1} & 0 & \bar{F}_{21}^{-1} & 0 \\ 0 & \bar{F}_{22}^{-1} & 0 & \bar{F}_{12}^{-1} \\ \bar{F}_{12}^{-1} & \bar{F}_{21}^{-1} & \bar{F}_{22}^{-1} & \bar{F}_{11}^{-1} \end{bmatrix} \quad (21)$$

NUMERICAL EXAMPLES

Helmholtz Equation

To evaluate the performance of the proposed method, the Helmholtz equation is solved. In general, the Helmholtz equation considers the wave equation for cases where all data are simple-harmonic. The Helmholtz equation admits the family of localized asymptotic solutions, which are globally free of singularities, and usually provides an effective tool to study the integration representation of high frequency wave fields.

In this research, we consider the following one-dimensional Helmholtz equation with dimensionless unit given by

$$\nabla^2 u(x) + k^2 u(x) = 0, \text{ on } \Omega = \{x | 0 \leq x \leq 2.5\} \quad (22)$$

with Dirichlet boundary conditions.

$$u(0) = 1, u(2.5) = 0 \quad (23)$$

where ∇^2 is the Laplacian, k is the wave number. For imaginary k , the equation becomes the spatial part of the diffusion equation. For real k , the solution of Helmholtz equation represents the spatial part of the wave equation. When k is zero, the equation reduces to the Laplace equation.

In this example, twelve uniformly distributed particles with the wave number equal to one and three are studied respectively. The particle number is chosen such that the discretization is close to the Nyquist limit and waves are allowed to propagate. The effect of the mesh-free approximation order is also considered. For the basis function order of one, normalized kernel function support of 1.5 is used; for the basis function order of two, normalized support of 2.5 is used. Comparisons between the consistent mass and lumped mass formulations are made.

When the wave number is one, the displacements obtained from the consistent mass and lumped mass formulations match the analytical solution very well for two different approximation orders as shown in Figure 2. The square symbol denotes the results with the consistent mass formulation, the triangular symbol represents the results with the lumped mass formulation, and the solid line is the analytical solution.

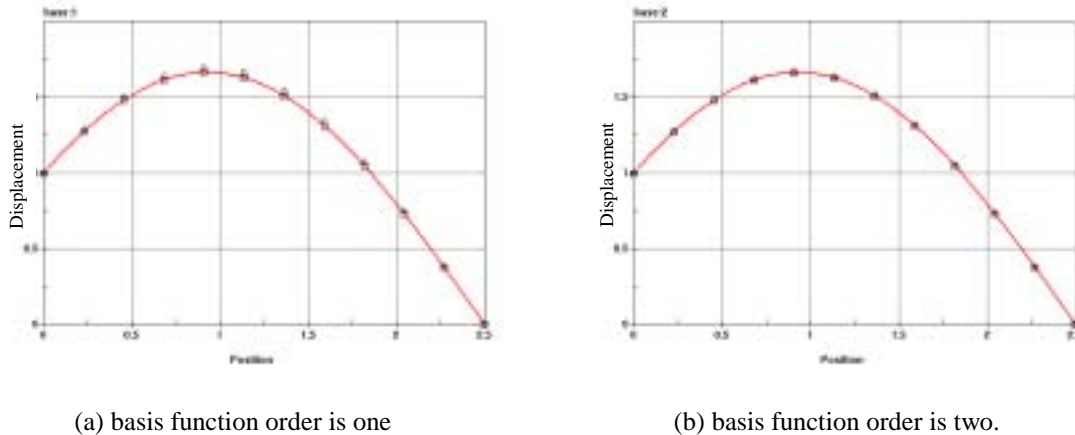


Figure 2. Displacement comparisons between consistent mass and lumped mass when the wave number is equal to one

Figure 3 shows, for higher wave number ($k = 3$) with approximation order equal to one, the consistent mass formulation still provides good performance whereas the solution obtained from the lumped mass loses some accuracy. By adding more particles, the discretization error in the lumped mass method could be minimized. Alternatively, the accuracy could also be improved by using higher order basis functions as shown in Figure 3 (b).

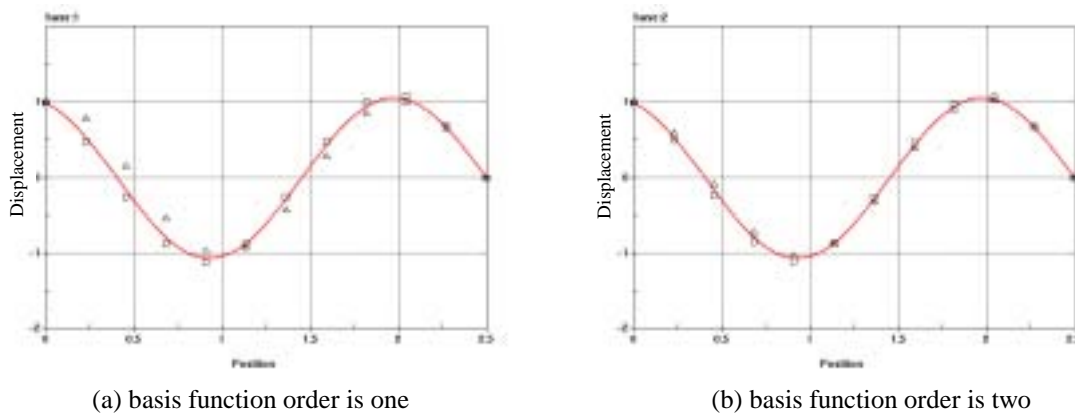


Figure 3. Displacement comparisons between consistent mass and lumped mass when the wave number is equal to three

Frictional Forging

This problem is studied to identify the applicability of the coupled finite element and mesh-free method to path-dependent materials with frictional contact conditions. A metal work piece compressed by a cylindrical punch as described in Figure 4 is analyzed. The plane-strain condition is considered. The punch is treated as a rigid body, and only the work piece is considered to be deformable. The material properties of the work piece are: initial density = $10E-3 \text{ lbf} \cdot \text{s}^2 / \text{in}^4$, Young's modulus = $6.825E7 \text{ psi}$, Poisson's ratio = 0.3 , and $J2$ perfect plasticity with yield stress = 6000.0 psi . The friction coefficient between the work piece and punch is assumed to be 0.2 . The velocity for the punch is 0.01 in/s . One mesh-free zone and the corresponding interface are added into the finite element based analysis model. Conventional finite element analysis is also conducted for comparison.

The analysis by the finite element method fails when severe mesh distortion occurs near the corner of the cylindrical punch as shown in Figure 4. The corresponding effective plastic strain is plotted in Figure 5. It is shown that finite element analysis displays a high level of effective plastic strains due to the tangled elements. As a result, a high level of stress concentration is expected in the conventional finite element analysis. On the other hand, the coupled finite element and mesh-free method effectively avoids the mesh tangling and provides smooth strain and stress distribution as shown in Figure 4 and 5. The progressive deformation obtained from the coupled finite element and mesh-free method is illustrated in Figure 6.

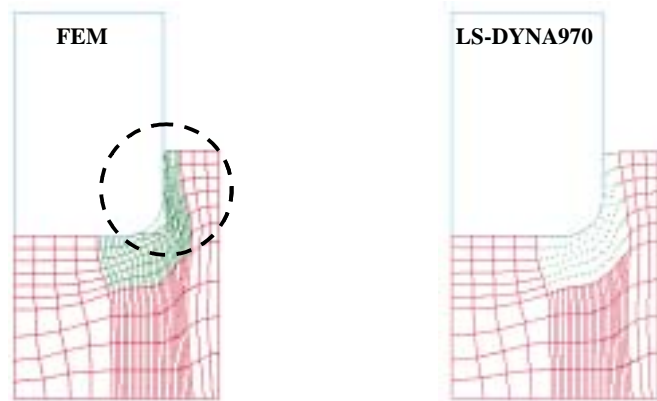


Figure 4. Comparison of deformed shapes.

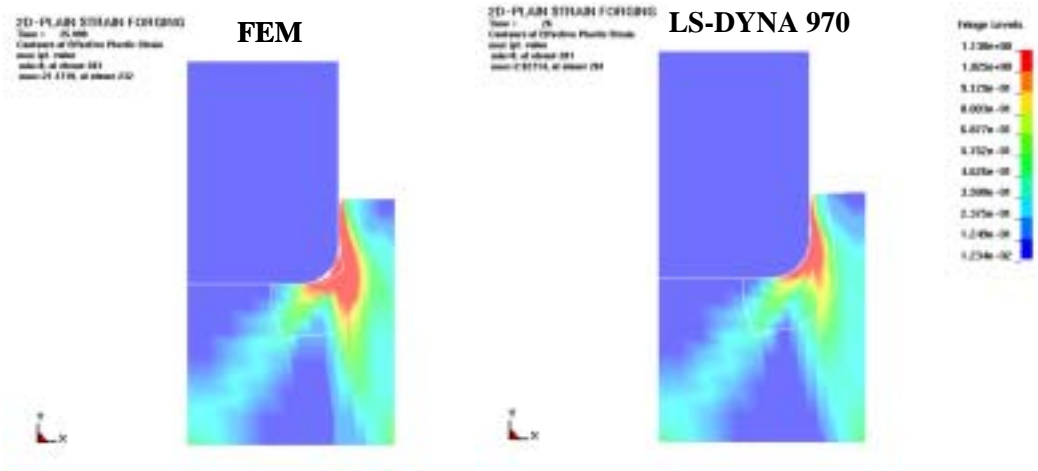


Figure 5. Comparison of effective plastic strain distribution.

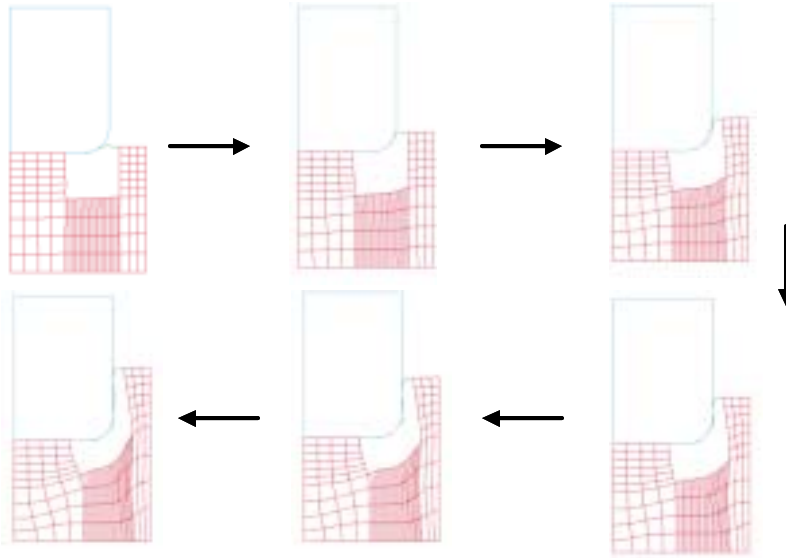


Figure 6. Progressive deformation by LS-DYNA 970.

CONCLUSION

To efficiently assess structural survivability, reusability and manufacturing for the industrial applications using simulation technology, a coupled finite element and mesh-free computational method is proposed for effective and realistic simulation of severe material deformation in structures.

To couple the mesh-free method with LS-DYNA, an *interface constraint* has been developed. To satisfy the linear exactness in the mesh-free Galerkin approximation of the Dirichlet boundary value problem, two *integration constraints* have been developed. A local boundary integration scheme with the coupled finite element and mesh-free shape function has been developed to satisfy the two *integration constraints*, to eliminate the possible hourglass modes and to reduce the computation time on the imposition of essential boundary conditions.

This method has been shown to perform well for explicit dynamics problems. The extension of this method to implicit analysis and shell formulation is under investigation.

ACKNOWLEDGEMENT

The support for this work by General Motors Corporation under contract TCS-12002 to LSTC is gratefully acknowledged.

REFERENCES

1. Babuska, I. and Melenk, J. M. (1996). "The Partition of Unity Method." *Int. J. Numer. Meth. Eng.*, Vol. 40, pp-727-758.
2. Belytschko, T., Lu, Y. Y. and Gu, L. (1994). "Element-Free Galerkin Methods." *Int. J. Numer. Meth. Eng.*, Vol. 37, pp-229-256.
3. Belytschko, T., Organ, D., and Kronggauz, Y. (1995). "A Coupled Finite Element- Element-Free Galerkin Method." *Computational Mechanics*, Vol. 51, pp-221-258.
4. Belytschko, T., Guo, Y., Liu, W. K., and Xiao, S. P. (2000). "A Unified Stability Analysis of Meshless Particle Methods." *Int. J. Numer. Meth. Eng.*, Vol. 48, pp-1359-1400.
5. Chen, J. S., Pan, C., Wu, C. T. and Liu, W. K. (1996). "Reproducing Kernel Particle Methods for Large Deformation Analysis of Nonlinear Structures." *Comput. Meth. Appl. Mech. Engng.*, Vol. 139, pp-195-227.
6. Chen, J. S. and Wang, H. P. (2000). "Some Recent Improvements in Meshfree Methods for Incompressible Finite Elasticity Boundary Value Problems with Contact." *Computational Mechanics*, Vol. 25, pp-137-156.
7. Chen, J. S. and Wang, H. P. (2000). "New Boundary Condition Treatments for Meshless Computation of Contact Problems." *Comput. Meth. Appl. Mech. Engng.*, Vol.187, pp-441-468.
8. Chen, J. S., Wu, C. T. and Belytschko, T. (2000). "Regularization of Material Instabilities by Meshfree Approximations with Intrinsic Length Scales." *Int. J. Numer. Meth. Eng.*, Vol. 47, pp-1303-1322.
9. Chen, J. S., Wu, C. T., Yoon, S., and You, Y. (2001). "A Stabilized Conforming Nodal Integration for Galerkin Meshfree Methods." *Int. J. Numer. Meth. Eng.*, Vol. 50, pp-439-466.
10. Chen, J. S., Yoon, S. and Wu, C. T. (2002). "Nonlinear Version of Stabilized Conforming Nodal Integration for Galerkin Meshfree Methods." *Int. J. Numer. Meth. Eng.*, Vol. 52, pp-2587-2615.
11. Hallquist, J. O. (2002). "LS-DYNA." Livermore Software Technology Corporation.
12. Huerta, A. and Fernandez-Mendez S. (2000). "Enrichment and Coupling of the Finite Element and Meshless Methods." *Int. J. Numer. Meth. Eng.*, Vol. 48, pp-1615-1636.
13. Liu, W. K., Jun, S., and Zhang, Y. F. (1995). "Reproducing Kernel Particle Methods." *Int. J. Numer. Meth. Fluids*, Vol. 20, pp-1081-1106.
14. Liu, W. K., Jun, S., Li, S., Adee, J., and Belytschko, B. (1995). "Reproducing Kernel Particle Methods for Structural Dynamics." *Int. J. Numer. Meth. Eng.*, Vol. 38, pp-1655-1679.
15. Liu, W. K., Uras R. A. and Chen, Y. (1997). "Enrichment of the Finite Element Method with Reproducing Kernel Particle Methods." *Journal of Applied Mechanics*, Vol. 64, pp-861-870.
16. Wagner, G. J. and Liu, W. K. (2000). "Application of Essential Boundary Conditions in Mesh-free Methods: A Corrected Collection Method," *Int. J. Numer. Meth. Eng.*, Vol. 47, pp-1367-1379.
17. Wu, C. T., Chen, J. S., Chi, L. and Huck, F. (2001). "A Lagrangian Meshfree Formulation for Analysis of Geotechnical Materials." *Journal of Engineering Mechanics*, Vol. 127, pp-440-449.
18. Wu, C. T. (2002). "Improvements of Mesh-free Galerkin Method for Structural Analysis." Internal Report, LSTC.